



TITAN'S UPPER ATMOSPHERE FROM CASSINI/UVIS SOLAR OCCULTATIONS

Fernando Javier Capalbo, Yves Bénilan, Roger V. Yelle, Tommi T. Koskinen

► To cite this version:

Fernando Javier Capalbo, Yves Bénilan, Roger V. Yelle, Tommi T. Koskinen. TITAN'S UPPER ATMOSPHERE FROM CASSINI/UVIS SOLAR OCCULTATIONS. *Astrophysical Journal*, American Astronomical Society, 2015, 814 (2), pp.86. <<http://iopscience.iop.org/article/10.1088/0004-637X/814/2/86>>. <10.1088/0004-637X/814/2/86>. <hal-01228946>

HAL Id: hal-01228946

<https://hal.archives-ouvertes.fr/hal-01228946>

Submitted on 15 Nov 2015

HAL is a multi-disciplinary open access archive for the deposit and dissemination of scientific research documents, whether they are published or not. The documents may come from teaching and research institutions in France or abroad, or from public or private research centers.

L'archive ouverte pluridisciplinaire **HAL**, est destinée au dépôt et à la diffusion de documents scientifiques de niveau recherche, publiés ou non, émanant des établissements d'enseignement et de recherche français ou étrangers, des laboratoires publics ou privés.



Distributed under a Creative Commons Attribution - NonCommercial - ShareAlike 4.0 International License

1 **TITAN'S UPPER ATMOSPHERE FROM CASSINI/UVIS SOLAR**
2 **OCCULTATIONS**

3 Fernando J. Capalbo and Yves Bénilan

4 Laboratoire Inter-Universitaire des Systèmes Atmosphériques (LISA), UMR 7583 du CNRS,
5 Universités Paris Est Créteil (UPEC) and Paris Diderot (UPD), 61 avenue du Général de Gaulle,
6 94010, Créteil Cédex, France

7 `fernando.capalbo@lisa.u-pec.fr`

8 and

9 Roger V. Yelle and Tommi T. Koskinen

10 Lunar and Planetary Laboratory, University of Arizona, 1629 E. University Blvd., AZ 85721,
11 Tucson, USA

12 Received _____; accepted _____

Submitted to Astrophysical Journal on 2015 July 22.

ABSTRACT

Titan’s atmosphere is composed mainly of molecular nitrogen, methane being the principal trace gas. From the analysis of 8 solar occultations measured by the Extreme Ultraviolet (EUV) channel of the Ultraviolet Imaging Spectrograph (UVIS) onboard Cassini, we derived vertical profiles of N₂ in the range 1100 - 1600 km and vertical profiles of CH₄ in the range 850 - 1300 km. The correction of instrument effects and observational effects applied to the data are described. We present CH₄ mole fractions, and average temperatures for the upper atmosphere obtained from the N₂ profiles. The occultations correspond to different times and locations, and an analysis of variability of density and temperature is presented. The temperatures were analyzed as a function of geographical and temporal variables, without finding a clear correlation with any of them; although a trend of decreasing temperature towards the north pole was observed. The globally averaged temperature obtained is (150 ± 1) K. We compared our results from solar occultations with those derived from other UVIS observations, as well as studies performed with other instruments. The observational data we present confirm the atmospheric variability previously observed, add new information to the global picture of Titan’s upper atmosphere composition, variability and dynamics, and provide new constraints to photochemical models.

Subject headings: occultations, planets and satellites: atmospheres, planets and satellites: composition, planets and satellites: individual (Titan), techniques: imaging spectroscopy

1. INTRODUCTION

1 Titan’s atmosphere hosts complex organic chemistry processes started by the ionization and
2 dissociation of molecular nitrogen (N_2), which accounts for more than 90% of the atmosphere, and
3 methane (CH_4), the main trace gas with variable abundance of a few percent. Knowledge of the
4 distribution of these constituents with altitude, latitude, and longitude is key to constraining the
5 atmospheric structure and dynamics, and thereby investigating energy and momentum balance
6 in the upper atmosphere. This knowledge is used to develop and constrain models investigating
7 atmospheric chemistry, aerosol production, thermal balance, and escape processes. Therefore,
8 independent, accurate, and precise determination of nitrogen and methane densities in the upper
9 atmosphere is of primary importance.

11 Several observations and techniques can be used to retrieve the densities of N_2 and CH_4 in
12 the upper atmosphere. One technique uses UV airglow measurements from the Cassini Ultraviolet
13 Imaging Spectrograph (UVIS) (Stevens et al. 2011, 2015). However, these results have a vertical
14 resolution of about 100 km and are dependent on the accurate knowledge of the instrument
15 function and radiometric calibration of UVIS, which has an uncertainty of $\sim 15\%$ (Stevens et al.
16 2011). The analysis of airglow data also depends on a complex model of the emission processes
17 of N_2 . Another technique uses atmospheric emissions in the infrared. García-Comas et al.
18 (2011) modeled CH_4 emissions and, comparing their model to limb observations performed by
19 the Cassini/Visual-Infrared Mapping Spectrometer (VIMS), derived methane abundances in the
20 range 500 - 1100 km. Again, these results depend on a sophisticated non-local thermodynamic
21 equilibrium model of methane emissions, and are subject to systematic uncertainties that
22 add to the statistical uncertainties in the retrieved profiles. On the other hand, in-situ mass
23 spectrometry, stellar, and solar occultations measured from a spacecraft are the most direct
24 measurements of Titan’s neutral upper atmospheric composition, providing a method to directly
25 probe N_2 densities. Several tens of N_2 and CH_4 profiles were measured ‘in-situ’ by the Cassini
26 Ion and Neutral Mass Spectrometer (INMS) (see for example Waite et al. 2005; Cui et al. 2009;
27 Snowden et al. 2013). The regularity of the close Titan flybys makes this type of observation the
28 most abundant source of information about the densities in the upper atmosphere. Unfortunately,

1 the spatial spread of the spacecraft trajectory in the atmosphere, together with the variability
 2 of the atmosphere, can be a disadvantage when interpreting the profiles in terms of geophysical
 3 variables (Mueller-Wodarg et al. 2008). Until recently there were uncertainties about the absolute
 4 magnitude of the N_2 densities in the upper atmosphere, with disagreement among values inferred
 5 from *in situ* measurements by INMS (Cui et al. 2009; Magee et al. 2009), from accelerometer
 6 measurements by the Huygens Atmospheric Structure Instrument (HASI, Fulchignoni et al. 2005),
 7 and from the Attitude and Articulation Control System (AACS) on the Cassini spacecraft (Sarani
 8 2009). The fact that the densities from INMS are systematically smaller by about a factor 3 from
 9 HASI and AACS pointed to a need to re-calibrate the INMS observations (Teolis et al. 2015).

10 Cassini/UVIS observes stellar and solar occultations in the EUV, which can be used to
 11 measure line of sight absorption by N_2 and CH_4 . Kammer et al. (2013) analyzed 4 UVIS/EUV-
 12 stellar occultations (flybys T21, T35, T41-I, and T41-II) and determined CH_4 and N_2 atmospheric
 13 profiles between 1000 and 1400 km by using an optimized grid search retrieval method. This
 14 method allowed them to determine the reduced χ^2 surface of the column densities, and is therefore
 15 convenient for estimating their uncertainty, before deriving number densities from them. Stellar
 16 EUV occultations, however, are limited by Inter Stellar Medium (ISM) absorption to wavelengths
 17 longward of 912 Å, where absorption is by highly complex N_2 electronic band systems (Lewis
 18 et al. 2008). These are difficult to interpret at the relatively low UVIS spectral resolution, as all
 19 the sharp lines must be modeled before convolution with the instrument function. Moreover, the
 20 low stellar flux (compared with the solar flux) leads to relatively low signal-to-noise ratio (S/N).

21 Solar occultations are a valuable method to retrieve the composition of the upper atmosphere.
 22 The first solar occultation by Titan was measured by the UVS instrument (Broadfoot et al. 1977)
 23 onboard the Voyager 1 spacecraft. This instrument covers the wavelength range 500 - 1700 Å
 24 and has a resolution of 10 Å. Although UVS measured an ingress and an egress occultations, the
 25 analysis of Smith et al. (1982) concentrated on the ingress leg because it had better geometrical
 26 characteristics. They used the data to confirm that the atmosphere is composed mainly of N_2 ,
 27 with a small abundance of CH_4 . Their results were used to constrain several subsequent models of
 28 the upper atmosphere (e.g., Yung et al. 1984; Lara et al. 1996; Yelle et al. 1997). A reanalysis of
 29 the Voyager solar occultation, utilizing a more sophisticated analysis technique and an improved

1 model of the instrument (Vervack et al. 2004), solved some inconsistencies noted by Strobel et al.
2 (1992) in the Smith et al. (1982) opacity profiles. Vervack et al. (2004) retrieved number density
3 profiles for N_2 , CH_4 , and other minor hydrocarbons. They used the continuum N_2 absorption
4 cross section below 650 Å to retrieve molecular nitrogen because the longer wavelength region
5 presenting strong absorption bands was not well known at that time. From the N_2 profiles Vervack
6 et al. (2004) derived a mean thermospheric temperature of 153 K. Cassini/UVIS solar occultations
7 observed in the EUV measure absorption in the ionization and dissociation continuum of N_2
8 and the dissociation region of CH_4 , where cross sections vary smoothly with wavelength and
9 have been precisely measured in the laboratory. Data corresponding to these absorption regions
10 are therefore relatively straightforward to analyze (after the instrument corrections detailed in
11 Section 2) and should provide reliable results. The higher spectral resolution of UVIS compared
12 to UVS allows to better identify and use solar features for the retrieval. A closer observation
13 and better spacecraft stability (except for observations with pointing instabilities) provide better
14 altitude resolution and reduce the corrections needed when processing the data with respect to
15 Voyager 1/UVS. The small spread in latitude/longitude of the observations allows to associate the
16 derived vertical profiles with precise geographical coordinates. Thus, based on a simple technique
17 (when compared with those used to the analysis of Titan’s airglow), using well known absorption
18 features, and being independent of calibration, UVIS solar occultations in the continuum region
19 of the absorption cross sections are among the most reliable methods to retrieve local density
20 profiles of N_2 , CH_4 , and temperatures in the upper atmosphere of Titan.

21 In this work we present number density profiles of N_2 , CH_4 , and temperatures in the
22 thermosphere of Titan, retrieved from 8 solar occultations observed by Cassini/UVIS during
23 the flybys T10, T26, T53, T58, T62 (ingress and egress), and T78 (ingress and egress). These
24 observations cover the period from January 2006 to September 2011. The solar occultation
25 from T53 was analyzed by Capalbo et al. (2013), the first published results from UVIS solar
26 occultations. In Section 2 of the present work we detail instrument corrections and data analysis,
27 including a correction of effects of unstable pointing that, if not corrected, would render some
28 of the observations unusable. Section 3 presents the occultations analyzed, including their
29 temporal and spatial coverage. The results are presented in Section 4, followed by a summary

1 and conclusions in Section 5.

2. UVIS SOLAR OCCULTATION ANALYSIS

3 A solar occultation occurs when the Sun, as viewed from Cassini, rises from or sets into
 4 Titan’s atmosphere. This type of observation has been described before (see for example Smith
 5 & Hunten 1990; Vervack et al. 2004; Capalbo 2014). From the transmission measured during an
 6 EUV occultation, information about the atmospheric composition can be derived for altitudes
 7 from 850 to 1600 km, which cover the thermosphere of Titan, near and above the homopause
 8 (850 - 1000 km, Vervack et al. 2004; Yelle et al. 2008; Cui et al. 2009). The ionization and
 9 dissociation of N_2 and CH_4 happen in this region, where the detection of less abundant molecules
 10 is prevented by strong absorption by these species in the UVIS/EUV range (561 - 1182 Å).

11 The first step in the analysis is to determine the geometric conditions for the observation.
 12 The spacecraft trajectory and attitude during the occultation are obtained with the help of SPICE
 13 kernels and ICY Toolkit (Acton 1996). Important geometrical information is given in Table 1.
 14 The distance from the spacecraft to Titan, the integration duration, and the spacecraft velocity
 15 and attitude determine the vertical sampling of the atmosphere. Integration time is 1 s for all
 16 solar occultations analyzed here. The distance from the spacecraft to the center of Titan and
 17 from the spacecraft to the tangent altitude point range from 10^3 to 10^5 km (the tangent altitude
 18 is the shortest distance from the surface of Titan to the line of sight from the spacecraft to the
 19 Sun). As a consequence, the vertical sampling varies between approximately 1 km to about 5 km.

20 In addition to the general steps in the UVIS data analysis described in the Cassini/UVIS
 21 User’s Guide (LASP 2014) available through the NASA Planetary Data System (PDS), some
 22 particular procedures are necessary to analyze UVIS EUV solar occultations. These procedures
 23 are described in Capalbo et al. (2013), and thoroughly explained in Capalbo (2014). Thus, we
 24 only mention relevant information from these references. It is worth noting that although all the
 25 solar occultations have common general characteristics and a common analysis protocol could
 26 be established, all present particularities that complicate the study, calling for a detailed case
 27 by case analysis. In particular, the position, size, and stability of the image of the source on

1 the detector. The angular size of in the FOV during the flybys is about 1 mrad. The perceived
 2 size of the Sun in the atmosphere level (about 1 - 25 km) is for most occultations bigger than
 3 the altitude sampling interval (see Table 1). This oversampling of the atmosphere allows binning
 4 the data in altitude (each resulting value being the average of the values in the bin) to improve
 5 S/N. The resulting effective sampling of the atmosphere is around 10 - 16 km, depending on the
 6 occultation.

7 2.1. Data Corrections

8 The most important corrections to the solar port data of the EUV channel are the background
 9 subtraction and, for observations with problematic pointing, the wavelength registration. These
 10 corrections were performed separately for each of the two spatial lines on the detector containing
 11 the solar image, after the onboard binning and before adding the signal in the lines. There are
 12 many sources of background. The Radio Thermal Generator background (henceforth BKG1) can
 13 be neglected. The present analysis accounts for contributions of photons coming from sources
 14 other than the Sun (BKG2), and from light dispersed by the grating (BKG3.1) and by internal
 15 reflections (BKG3.2). The contribution of BKG2 was estimated from observations made when all
 16 solar light is completely extinguished by atmospheric absorption (altitudes $\lesssim 300$ km), giving for
 17 all occultations a negligible contribution at a rate of a few 10^{-2} counts sec^{-1} pixel^{-1} . Although
 18 the exact source, spectral and time variation of the scattered light contribution (BKG3.1 and
 19 BKG3.2) are unknown, the spectral and temporal characteristics of the data reveal the presence
 20 of at least two distinct contributions. The first varies with time in the same manner as the count
 21 rate at the long wavelength end of the spectrum. This can be seen in Figure 1, showing light
 22 curves from the T53 occultation for bins around solar lines at 584 \AA and 630 \AA , and for a bin
 23 covering the range $1100 - 1160 \text{ \AA}$. For altitudes below ~ 1000 km, the light curve for the short
 24 wavelength bins show background counts that vanish in a similar fashion to that of the counts
 25 in the long wavelength bin. It was therefore hypothesized that this background is due to light
 26 scattered by the instrument from longer wavelengths. We corrected it following the procedures
 27 described in Capalbo et al. (2013); Capalbo (2014). The second manifestation of the scattered

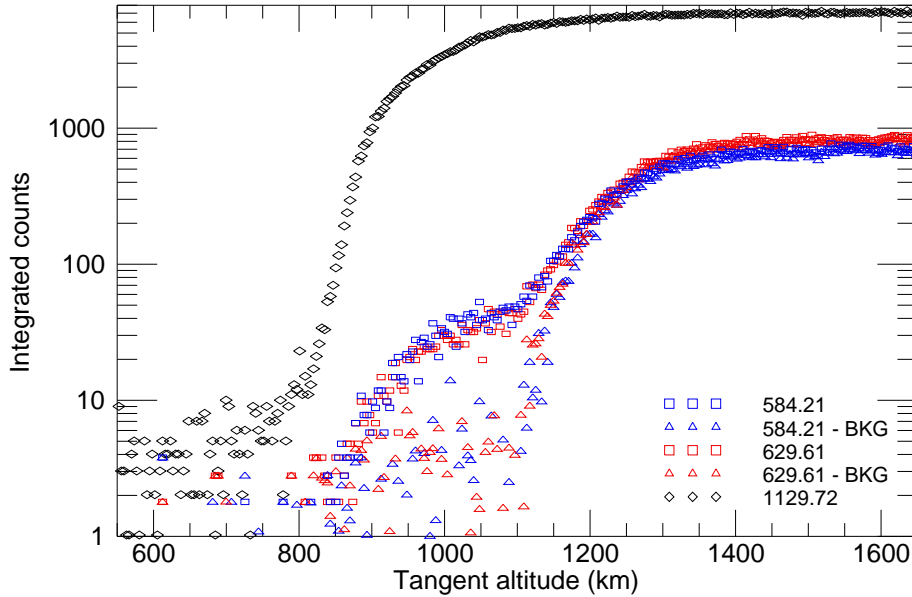


Fig. 1.— Light curves for 7-band bins centered in two solar lines before (\square) and after (\triangle) the BKG correction. Light curve for a 100-band bin in the long wavelength end of the detector (\diamond) used as proxy for one of the sources of BKG. The wavelengths corresponding to the center of the bins are shown in the plot, in \AA . The data are from the T53 flyby.

1 light is in the form of residual background evident next to the measured solar emission lines.
 2 Interpreted as extended wings of the instrument Point Spread Function (PSF), its temporal
 3 behavior is the same as that of the emissions features themselves. It had no effect on the analysis,
 4 so it was not subtracted. The corrected light curves for bins around 584 \AA and 630 \AA are shown
 5 in Figure 1.

6 A wavelength re-calibration was also necessary. Even when the Sun remained within the
 7 limits of the FOV for all the occultations, the Sun could be imaged off the slit center in the
 8 dispersion or spatial direction, and it could drift further during the observation due to pointing
 9 instabilities — examples of the calculated positions and sizes of the Sun in the FOV, in a case
 10 of good pointing (flyby T58) and in a case of bad pointing (flyby T62) are shown in Figure 2.
 11 This resulted in spectra suffering from a wavelength- and time-dependent shift with respect to
 12 the calibration provided in the PDS archive. This shift is significant for 4 of the 8 occultations
 13 analyzed here (see Section 3). Based on the position of well known and strong solar emission

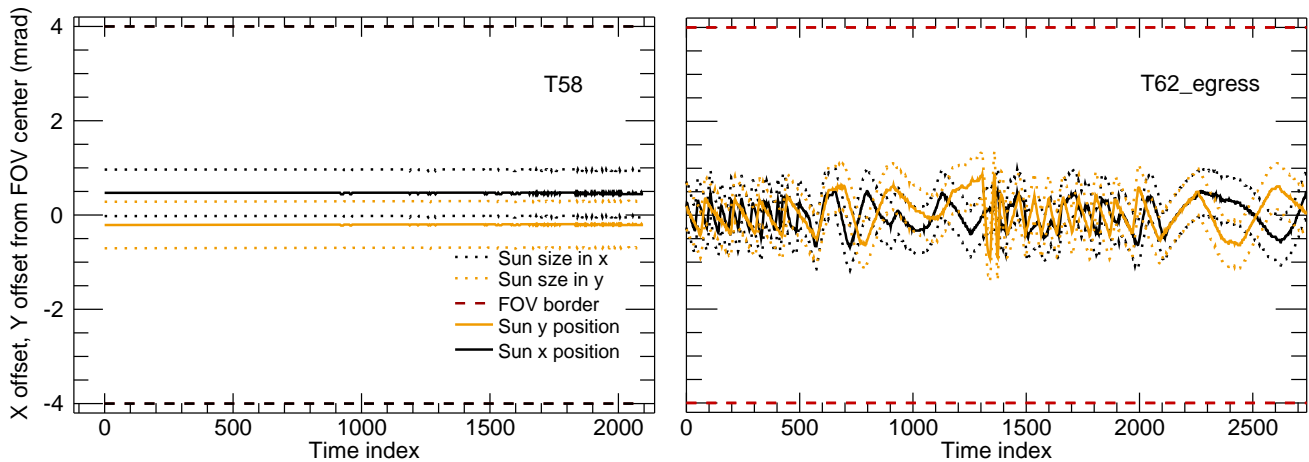


Fig. 2.— Sun position (solid lines) and size (dotted lines) in the across slit (X) dimension and along slit (Y) dimension of the squared FOV of the UVIS solar occultation port, for occultations T58 and the egress leg of T62. The difference time ranges are a consequence of the different duration of the occultations.

1 lines, a re-calibration of all measured spectra was performed. The drift of the solar image in the
 2 detector led to significant variations in the light curves as the flux of a solar emission line moved
 3 from one wavelength band to the other over time (see the top right panel of Figure 3). These
 4 UVIS bands were identified in the UVIS spectra as the center of a Gaussian fitted to the emission
 5 line. An example of this is shown in the bottom plots of Figure 3, showing the UVIS/EUV band
 6 corresponding to 629.61 \AA as a function of time, for detector line 5. As the movement of the
 7 spacecraft that originated the pointing drift is expected to be smoother than the oscillations
 8 observed, the data was smoothed as shown by the trend line in the plot (green solid line). For
 9 the lower altitudes, where the reference solar lines were absorbed, a quadratic extrapolation of
 10 the behavior at the higher altitudes was used. Once the position of the reference lines in terms of
 11 UVIS bands was determined, a wavelength calibration polynomial of second order was derived for
 12 each altitude. The measured wavelength shift for the reference lines vary from one occultation to
 13 the next, being 3.2 \AA (~ 5 pixels) in the worst case. The residual i.e., the difference between the
 14 wavelengths of the reference solar lines and the corrected wavelengths of the lines in the data, is
 15 up to 0.4 \AA in the worst case, but less than 0.2 \AA for most cases. This reflects the accuracy of
 16 the wavelength re-calibration, which is about $1/3$ of an EUV wavelength band.

1 The top plots in Figure 3 show the light curves before and after background and wavelength
 2 correction for the UVIS/EUV band 113 (corresponding to 629.61 \AA), for a stable (T53) and an
 unstable (egress leg of T62, henceforth T62_{egress}) occultation. In the case of T53, no perturbation

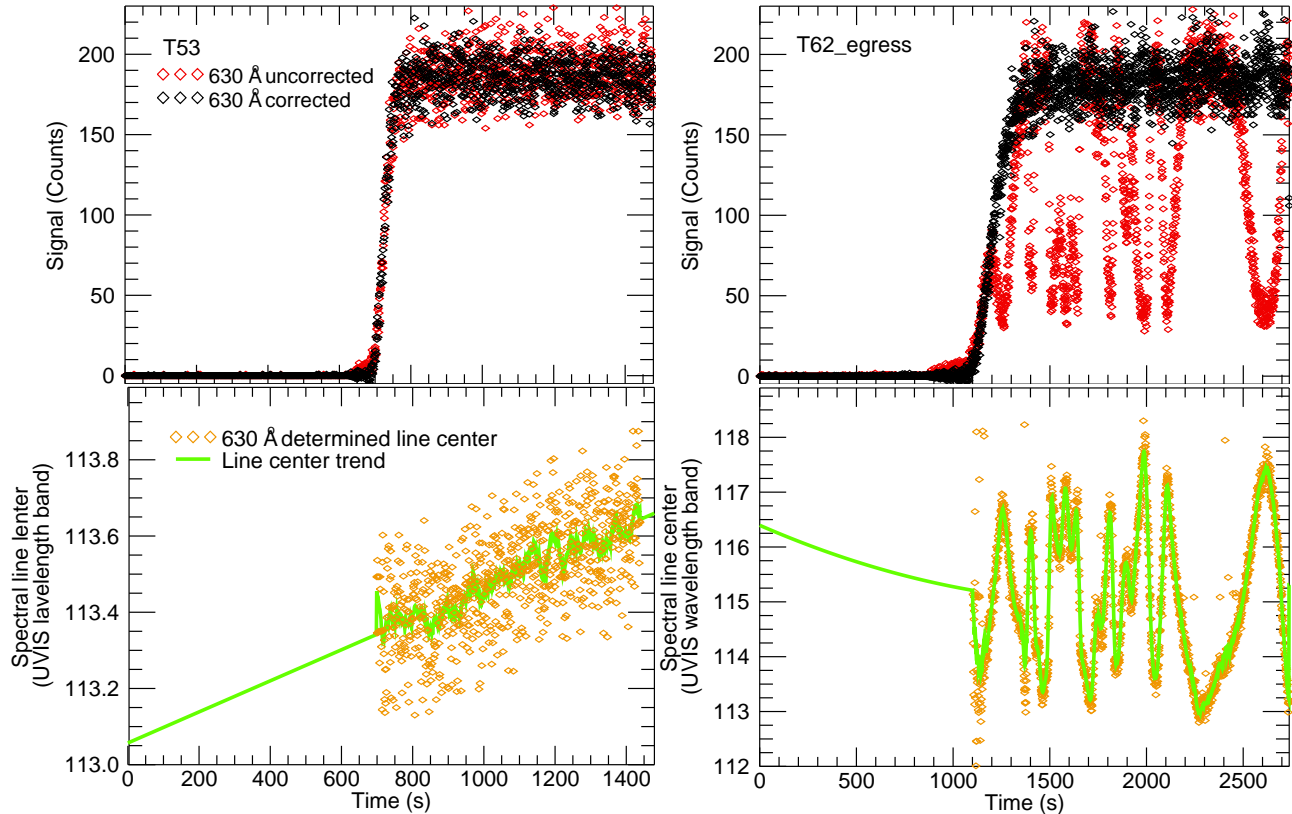


Fig. 3.— Top: Light curves before and after background and wavelength correction for UVIS/EUV band 113, corresponding to 629.61 \AA (representative of a solar emission line). Bottom: UVIS/EUV band corresponding to the 629.61 \AA emission line center (as determined from the Gaussian fits, see text), for detector line 5, as a function of observation time. The plots on the left and right correspond to the T53 and egress leg of T62 solar occultations, respectively.

3
 4 is clear from a visual inspection of the light curves, but the analysis shows a small, sub-pixel
 5 wavelength shift. For the unstable occultation the light curve is clearly corrupted by the shift.
 6 It has to be kept in mind that each observation has its own characteristics and these methods
 7 are more or less effective in each case. In cases with very bad pointing, one could wonder if the
 8 wavelength correction results in an acceptable light curve. This was confirmed by analyzing the
 9 statistics of the light curve above the Top Of the Atmosphere (TOA) for 2 of the most affected

1 occultations (T26 and T62_{egress}). Figure 4 shows the histogram of counts measured outside the
 2 atmosphere in the bins used for the analysis of absorption (582.40 - 586.03 Å, 627.79 - 631.43
 3 Å, and 1082.73 - 1087.58 Å), after the data corrections, for these ‘worse case’ occultations.
 The histograms for a stable occultation (T58) are also shown for comparison. The similarity of

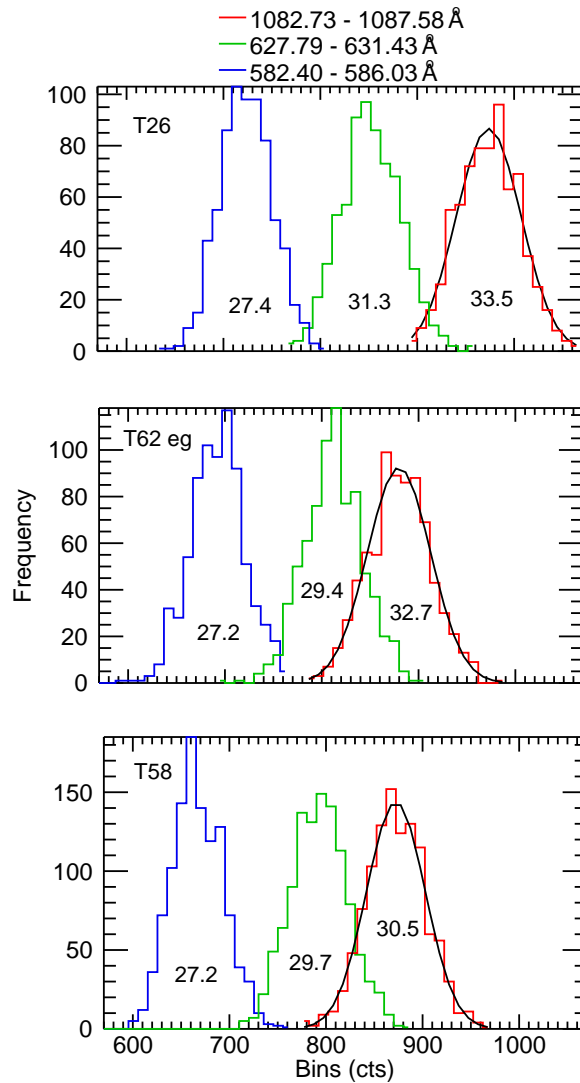


Fig. 4.— Count statistics above the atmosphere for the spectral bins shown at the top of the plot, for observations during flybys T26, T62_{egress}, and T58, after data corrections. The numbers in the plots are the standard deviations of the fitted Gaussians, one of which is shown as example in each plot.

4
 5 the histograms shows that the corrected light curves present similar statistics as those from an
 6 occultation with stable pointing. The re-calibration procedure not only confirms the correlation

1 of the fluctuations in the light curve with the shift of the line center in the detector—which also
 2 correlates with the pointing drifts shown in Figure 2—but also efficiently corrects the light curves.

3 2.2. Atmospheric Absorption and Analysis Methods

4 Nitrogen and methane are the main EUV absorbers in Titan’s atmosphere. Nitrogen, by far
 5 the dominant atmospheric constituent, absorbs photons in the region 561 - 1000 Å. Methane has a
 6 wider absorption region (561 - 1450 Å in UVIS/EUV,FUV ranges), and absorbs most photons in
 7 the remaining 1000 - 1450 Å wavelength range (see for example Lavvas et al. (2011) for a detailed
 8 description of N₂ and CH₄ absorption). The less energetic photons penetrate deeper into the
 9 atmosphere and can be absorbed by minor species (Koskinen et al. 2011). The Sun was assumed
 10 to have a steady output during the occultations. The EUV spectrum of the Sun consists of a weak
 11 continuum intercepted by intense emission lines. We retrieved density profiles of N₂ and density
 12 profiles of CH₄ by using two bins centered on the solar He I line at 584 Å (582.40 - 586.03 Å)
 13 and the O V line at 630 Å (627.79 - 631.43 Å), and a bin spanning solar lines around 1085 Å
 14 (1082.73 - 1087.58 Å), respectively. The retrieval procedure to calculate column densities and
 15 number densities is explained in Capalbo et al. (2013); Capalbo (2014). It takes advantage of the
 16 facts that CH₄ dominates absorption in the long wavelength bin, that N₂ dominates absorption
 17 in the short wavelength bins (although a CH₄ contribution is still important and accounted
 18 for, Capalbo et al. 2013; Capalbo 2014), and that the cross sections do not change significantly
 19 in the wavelength bins used. The procedure allowed us to retrieve abundances without using the
 20 complicated band structure in the N₂ absorption cross section, where the cross section varies by
 21 several orders of magnitude in narrow lines (Lewis et al. 2008). The N₂ absorption cross sections
 22 used for the calculations are from Samson et al. (1987), measured with a band-pass of 1 to 3 Å;
 23 the CH₄ absorption cross sections used are from Kameta et al. (2002), with resolution of 1 to 4 Å
 24 and measured at 298 K. The absorption cross sections have an uncertainty of ~ 3%.

25 The column density profiles were limited in altitude before the number density calculations.
 26 Column densities calculated for altitudes with very low, or too high absorption are affected by
 27 noise, background, and other measurement effects, and do not represent the real state of the

1 atmosphere. To limit the profiles, the valid altitudes for a particular profile were defined as those
 2 for which the transmission in the wavelength bin used for the retrieval satisfied:

$$T + \sigma_T < 0.99 \quad \text{and} \quad T - \sigma_T > 0.01, \quad (1)$$

3 where T and σ_T represent the transmission and its uncertainty, respectively. Nevertheless, values
 4 at the extremes of the resulting profiles deserved a special attention. Some values at the lowest
 5 altitudes in some of the nitrogen profiles seem to be too small, which could be due to residual
 6 background contamination not eliminated by the corrections described above. At the highest
 7 altitudes, the column densities showed a big dispersion and uncertainties. Moreover, at these
 8 high altitudes, the CH_4 contribution to the absorption at short wavelengths, used to correct the
 9 measured N_2 optical depth, is calculated using extrapolated CH_4 number densities (see Capalbo
 10 et al. 2013; Capalbo 2014), and therefore the resulting N_2 column densities are less precise. Thus,
 11 column densities with uncertainties bigger than 100% at the top of the profiles were excluded.
 12 The only exception was the profile calculated from the 584 Å bin for T26, values at 1492, 1508,
 13 and 1541 km had uncertainties bigger than 100% but were not the upper most values in the
 14 profile. Thus they were interpolated, assuming a decreasing exponential behavior as a function of
 15 altitude. This was done to keep as many high values as possible, and because the spatial inversion
 16 routines need a column density profile without missing values.

17 The retrieved number densities are very sensitive to oscillations in the column density
 18 profiles. After the regularized inversion, altitudes for which the inversion routine failed, resulting
 19 in negative number densities or with uncertainties bigger than 100%, were excluded from the
 20 profiles. This happened for only a few altitudes in the high end of the profiles. Values within one
 21 resolution width from the top of the profiles were eliminated, to avoid border effects due to the
 22 second derivative operator used in the inversion (Capalbo 2014). The N_2 number densities shown
 23 in Section 4 were calculated as the mean of the number densities derived from each bin involved in
 24 the analysis (centered in 584 Å or in 630 Å) for altitudes where the number densities overlapped.
 25 For altitudes with results from only one bin, this value was taken as the number density for that
 26 altitude. The different altitudes in the number density profile have similar, but different altitude
 27 resolutions, determined by the altitude sampling and the width of the averaging kernels of the
 28 inversion (see for example Capalbo et al. 2013). The median of the resolutions was calculated

1 as a characteristic resolution for the whole profile. The resolution for the average N_2 profile was
 2 calculated as the average of the resolutions of the profiles derived from the individual bins.

3 The N_2 number density profiles were used to derive temperature in the upper atmosphere of
 4 Titan. Nitrogen is relatively inert and, due to its dominance in the upper atmosphere, its average
 5 temperature can in general be regarded as a good indicator of the average temperature of the
 6 atmosphere as a whole. The procedure used to derive temperature is based upon the assumptions
 7 of a hydrostatic, diffusive and isothermal upper atmosphere. Under these assumptions, the
 8 temperature can be calculated from an effective scale height of the atmosphere, obtained from
 9 a linear fit to the natural logarithm of the measured number densities. This method has been
 10 used before to derive temperatures from INMS measurements (Cui et al. 2009; Westlake et al.
 11 2011). We derived temperature from the N_2 profile calculated as the mean of the number density
 12 profiles derived from each bin involved in the analysis (centered in 584 Å or in 630 Å). To avoid
 13 systematic uncertainties coming from values in the borders of the profiles (see comments on
 14 column densities above), the calculations were limited to altitudes for which the transmission in
 15 the wavelength bin used to retrieve the profile was between 0.1 and 0.9. In the rare cases when the
 16 altitudes were different for the two bins, the lower altitude between the two upper limits, and the
 17 higher altitude between the two lower limits were kept. The observation T62_{egress} is an exception.
 18 As the spacecraft was inside the atmosphere during part of the observation (see Section 3) the
 19 number densities are underestimated, especially for the highest altitudes, for which Cassini was
 20 deeper into the atmosphere. We therefore present two temperatures for this flyby. A lower limit
 21 for the temperature was calculated as for the other occultations, using the N_2 profile limited
 22 to the range 1144 - 1319 km. The other temperature was calculated using the profile from the
 23 lowest altitude retrieved up to 1144 km. For this observation, the densities at these low altitudes
 24 seem to be not affected by the issues mentioned above, and were therefore used to determine a
 25 ‘low altitude temperature’. Unless otherwise stated, it is this ‘low altitude temperature’ that is
 26 referred to when the temperature from this observation is considered.

27 We evaluated the uncertainty of the mean temperature by using a Monte Carlo technique.
 28 For each occultation we simulated 40000 number density profiles. For each simulated profile
 29 the number density for each altitude was drawn from a normal distribution with mean equal

1 to the value in the retrieved profile, and standard deviation equal to the retrieved uncertainty.
2 The uncertainties used for the simulated profiles were equal to the retrieved uncertainties. The
3 reported temperatures and uncertainties are obtained from the mean and standard deviation
4 of the temperatures obtained from the simulated profiles. The Monte Carlo analysis was also
5 performed with the individual profiles derived from the two short wavelength bins, and a
6 temperature was calculated as the mean of those derived from each profile. The results were
7 consistent with those obtained averaging the profiles and then calculating temperature.

8 3. UVIS OCCULTATIONS ANALYZED

9 We analyzed solar occultations through Titan’s atmosphere measured with the UVIS/EUV
10 channel that took place during flybys T10 through to T78. The data are available on the PDS
11 database. Geographical and other ancillary information about the solar occultations analyzed
12 in this work is presented in Table 1. When a range of values is given, the values are sorted by
13 increasing time of observation.

14 This final list merits some comments. In some cases an ingress occultation and an egress
15 occultation were measured during the same flyby. This is the case of T10, T62 and T78. The
16 ingress leg of T10 is unusable, the spacecraft was inside the atmosphere while the occultation took
17 place and the light curves are not appropriate for the analysis. The egress leg of T10 will therefore
18 be simply referred to as T10. The spacecraft was also inside the atmosphere during part of the
19 egress occultation that took place during the T62 flyby (T62_{egress}). Cassini’s altitude was lower
20 than 1500 km for tangent altitudes between approximately 1025 and 1450 km, passing by the
21 tangent altitude point when the tangent altitude was around 1350 km. Nevertheless, the resulting
22 light curves were suitable for analysis, and abundances could be derived. Obviously, as the line
23 of sight did not probe the whole atmosphere, the abundances derived should be considered lower
24 limits. The abundances at low altitudes, however, measured when Cassini was just entering the
25 atmosphere, are expected to be less underestimated than those at high altitudes.

26 Observations during T10, T26, and both observations during T62 suffered from pointing
27 instabilities causing wavelength shifts. In these cases the wavelength re-calibration procedure,

Table 1. Characteristics of solar occultations analyzed.

Flyby	Data product (EUVyyyy_doy_hh_mm)	Lat. ^a (deg)	Lon. ^a (deg W)	LST ^b (hh:mm)	SLT ^b (hh:mm)	Altitudes probed (km)	Original sampling ^a (km)	Sun diameter in atm. ^a (km)	Min. distance ^{d,a} (km)	T (K)
T10	EUV2006_015_11_25	-62 – -54	0 – 11	20:04	08:31	0 – 5365	2.6 – 2.9	9.7 – 11	9513	163 ± 2
T26	EUV2007_069_01_05	-76 – -77	41 – 29	23:10	13:47	10185 – 0	5.4 - 5.3	5.7 - 5.4	5293	139 ± 5
T53	EUV2009_110_00_11	-21 – -29	237	18:03	22:02	0 – 4802	3.9 – 4.3	5.1 – 4.7	4782	154 ± 5
T58	EUV2009_189_15_42	87 – 85	240 – 237	17:40	21:47	6663 – 0	3.2	12 – 11	10994	113 ± 4
T62 _{leg}	EUV2009_285_08_15	-68 – -61	48 – 49	06:08	21:35	0 – 2432	1.1 – 0.9	2.7 – 0.3	0	179 ± 9 ^c
T62 _{in}	EUV2009_285_06_27	2 – -5	230	17:59	21:31	5937 – 0	1.3 – 1.2	26 – 23	23108	172 ± 2
T78 _{leg}	EUV2011_255_02_23	25 – 20	354 – 352	05:41	17:32	0 – 7914	4.8 – 5.0	7.4 – 7.2	7450	160 ± 5
T78 _{in}	EUV2011_255_02_23	28 – 32	162 – 161	18:25	17:31	4021 – 0	5.0 – 4.8	9.4 – 9.2	9528	121 ± 3

^aFor altitudes relevant to CH₄ or N₂ absorption.

^bST: Titan's Local Solar Time. SLT: Saturn Local Time. For the half light point in the light curve of the bin around 584 Å.

^cow altitude value.

^dSpacecraft - tangent altitude minimum distance.

1 described in Section 2.1, allowed for the data to be corrected and column densities could be
 2 retrieved as usual. Although flybys T53, T58 and T78 were more stable and the correction was
 3 not critical, the wavelength correction was still performed to improve the quality of the data. The
 4 solar occultation measured during flyby T32 presented pointing instabilities that could not be
 5 corrected with the procedures use in this work, therefore no abundances were derived from it.

6 The geographical coordinates for relevant altitudes (in terms of absorption) of all the
 observations analyzed are summarized in Figure 5. The coordinates of the T53 UVIS/FUV-stellar

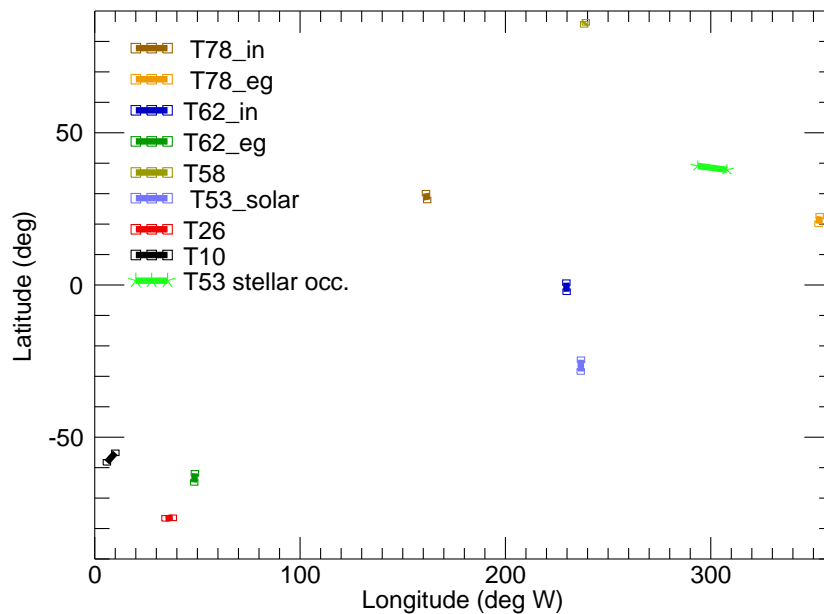


Fig. 5.— Latitude and Longitude for all the observations analyzed.

7
 8 occultation (Koskinen et al. 2011) is also shown. Although the latitude coverage is sparse, the
 9 occultations probed low, mid and high latitudes in both hemispheres. There are, however, gaps
 10 in the sampling, most of the occultations accumulating in low/mid latitudes on both hemispheres
 11 and longitudes above 150° W, or in high southern latitudes and longitudes below 100° W. The
 12 solar occultations also probe different longitudes, leaving big gaps for the longitude range 50 -
 13 150° W and for the range 250 - 350° W. Most of the solar occultations took place at the evening
 14 terminator, only 2 took place at the morning terminator. None of them took place while Titan
 15 was positioned from Saturn midnight to Saturn sunrise times.

4. RESULTS AND ANALYSIS

Figures 6 and 7 show the CH_4 and N_2 number densities, respectively. The profiles from

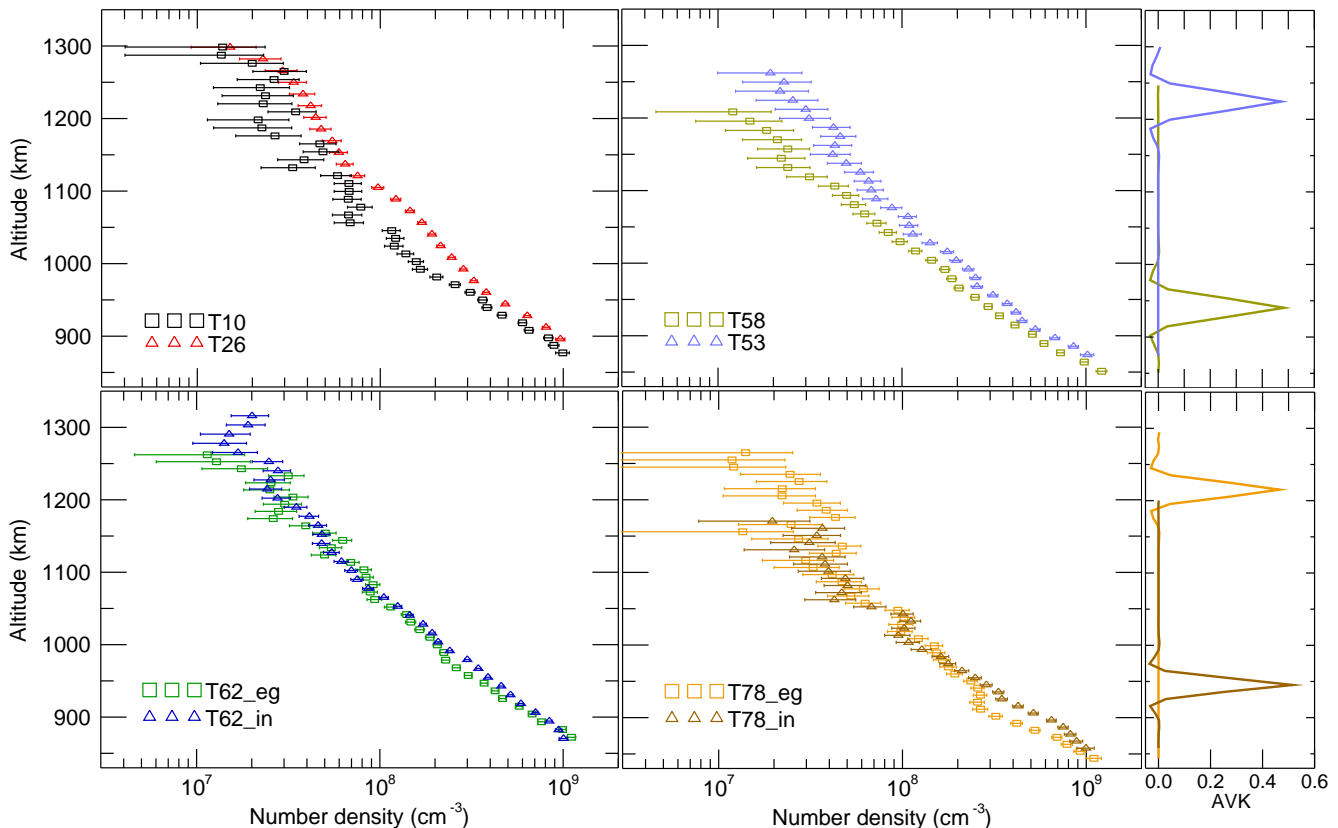


Fig. 6.— Methane number density profiles derived from the solar occultations analyzed. Densities from T62_{egress} above 1025 km should be interpreted as lower limits. On the right, as an example, AVK for some altitudes, and for four of the profiles: T53, T58, T78_{ingress}, T78_{egress}.

2
3 T53 were first presented in Capalbo et al. (2013). Most of the profiles present oscillations.
4 Atmospheric waves have been proposed to explain oscillations observed in CH_4 and N_2 density
5 profiles from Titan (see for example Koskinen et al. 2011; Snowden et al. 2013). The oscillations
6 in our results, especially those oscillations within a few tens of km, should be interpreted with
7 caution as they might be due to divergences from the real profile caused by the noise in the
8 column densities, not smoothed by the regularization procedure. The spacecraft was inside the
9 atmosphere during part of T62_{egress} (see Section 3). Therefore, the number densities, especially
10 in the upper part of the profiles, are underestimated and should be interpreted as lower limits.

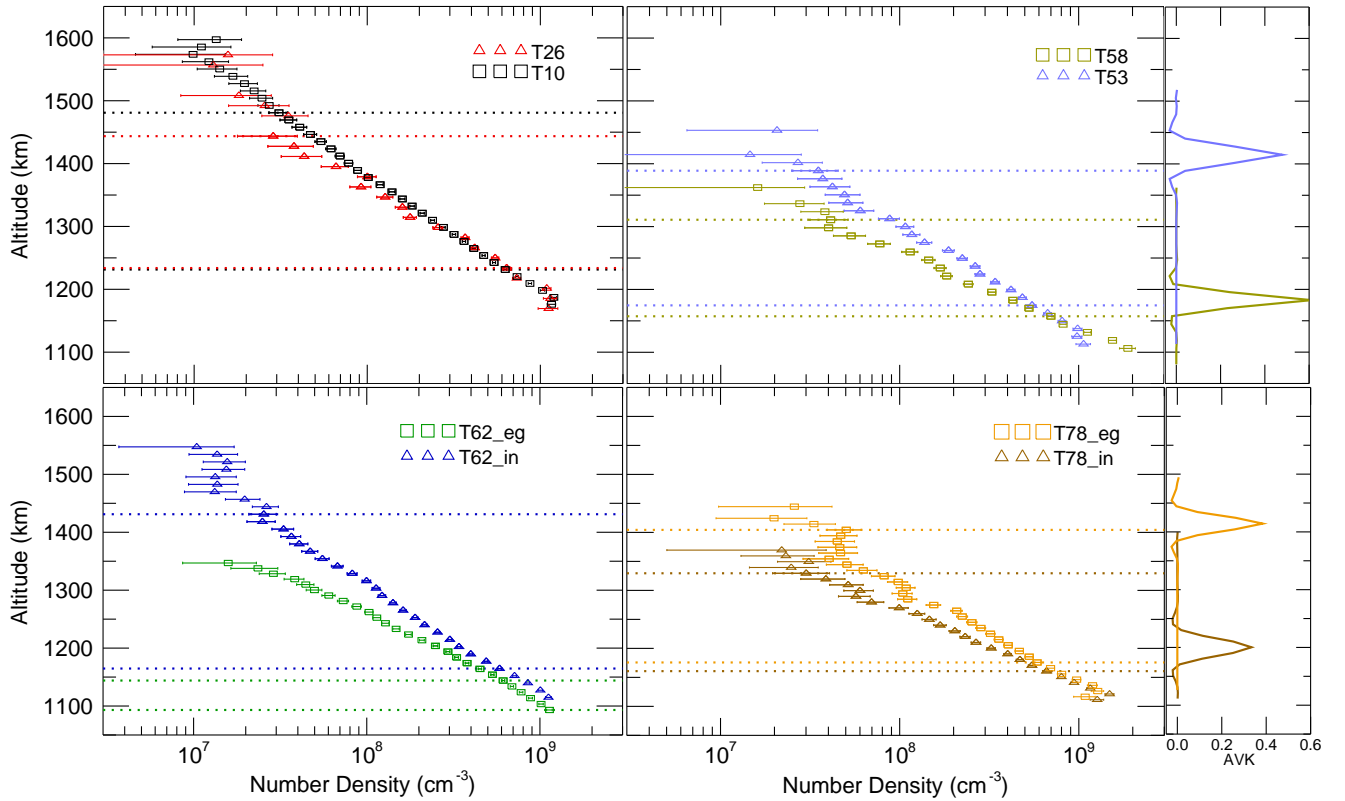


Fig. 7.— Nitrogen number density profiles derived from the solar occultations analyzed. Densities from $T62_{egress}$ should be interpreted as lower limits. The horizontal dotted lines show the altitude range used to derive temperature. On the right, as an example, AVK for some altitudes, and for four of the profiles: $T53$, $T58$, $T78_{ingress}$, $T78_{egress}$.

1 The altitude resolution of the profiles vary from one observation to the other. The resolution
2 associated with the CH_4 number densities is about 20 km for $T10$, $T62_{egress}$, $T78_{egress}$, and
3 $T78_{ingress}$, about 30 km for $T53$, $T58$, and $T62_{ingress}$, and about 50 km for $T26$. The resolution
4 associated to the N_2 number densities is about 20 km for $T26$ and $T58$, about 30 km for $T53$,
5 $T62_{egress}$, $T62_{ingress}$, $T78_{egress}$, and $T78_{ingress}$, and around 50 km for $T10$. The final altitude
6 resolution depends on the width of the averaging kernels (AVK). Averaging kernels for particular
7 altitudes are shown in Figures 6 and 7, as an example, for four of the occultations: $T53$, $T58$,
8 $T78_{ingress}$, $T78_{egress}$. The AVKs for N_2 correspond to the profiles derived from the 584 Å bin.

4.1. Number Density Variability

In the context of the variability observed in Titan’s thermosphere (see e.g. Magee et al. 2009; Snowden et al. 2013), it is interesting to analyze the behavior of the number densities measured. The solar occultation data confirm the variability observed in the upper atmosphere by other instruments, and are consistent with the decrease in densities over time observed in the INMS data. Even for profiles derived from one flyby but different occultations (e.g. T78), the profiles are clearly different.

Aiming at a quantitative analysis of variability, we concentrated on the number densities measured at 1250 km for N_2 and at 900 km and 1170 km for CH_4 . Table 2 shows statistics for the number densities corresponding to the altitudes in the profiles closest to the altitudes mentioned above. The high altitude value in the profile of methane from T62_{egress}, and the profile of nitrogen from the same flyby were not considered for the analysis of variability. The values in Table 2 indicate that the relative dispersion measured for nitrogen is more important than that measured for methane, and that the relative dispersion of methane sampled at low altitude is smaller than that sampled at high altitude. It has to be taken into account, however, that the different locations and times corresponding to the different observations are blended in this statistics.

Figure 8 shows the number densities for the selected altitudes, plotted as a function of time. In both the CH_4 and the N_2 data sets there is an overall tendency of decreasing abundance with time. The steepest decrease as a function of time is that of the values sampled at 900 km in the CH_4 profiles. It is worth noticing, however, that different locations are blended in this plot.

Table 2: Number Density Statistics.

Species	N_2	CH_4	
Altitude (km)	1250	900	1170
Median ($\times 10^7 cm^{-3}$)	22	68	4.6
Mean ($\times 10^7 cm^{-3}$)	28	68	3.7
Std. Dev. ($\times 10^7 cm^{-3}$)	16	20	1.5
Std. Dev./Mean	0.58	0.30	0.40

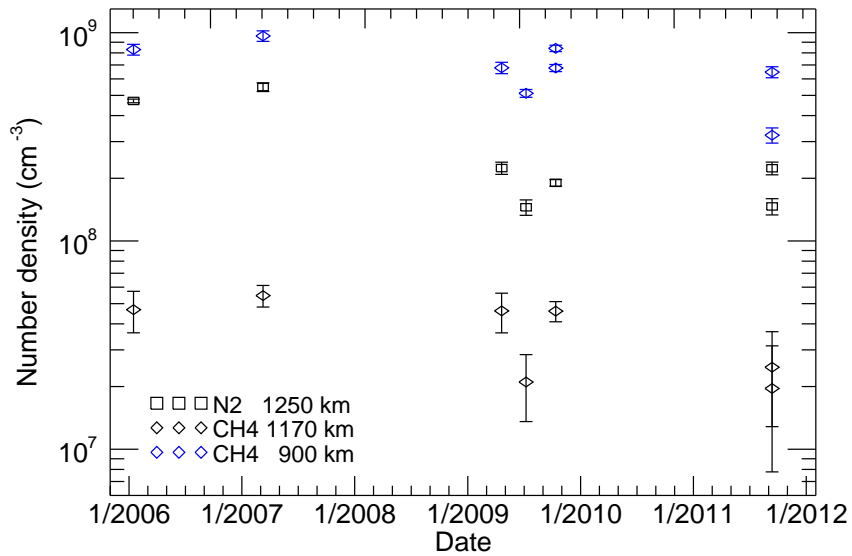


Fig. 8.— Methane number densities and nitrogen number densities versus time, for the three different altitudes shown in the plots.

1 A downward general trend of the N₂ densities during the Cassini mission has been observed by
 2 Westlake et al. (2014). In their analysis of INMS data from the TA-T95 flybys the highest densities
 3 observed were measured during the TA and T5 encounters and the lowest densities observed late
 4 in the mission. Snowden et al. (2013), in their analysis of INMS data from the T5-T71 flybys,
 5 observed that the median temperature in the upper atmosphere decreased after flyby T32, which
 6 took place in June 2007. This correlates with the decrease in N₂ densities in the present data
 7 set after T26, which took place in March 2007. Nevertheless, considering the limited sampling in
 8 the present work, the overlapping of uncertainties at high altitudes, and the oscillations in the
 9 density profiles, the trends described at the different altitudes should be interpreted with caution.

4.2. Methane Mole Fraction

10
 11 An important contribution of this work is the derivation of N₂ number density profiles and
 12 CH₄ number density profiles for the same time and location in the upper atmosphere. This
 13 allows for a straightforward determination of the vertical profile of the CH₄ mole fraction, an
 14 important quantity characterizing the dynamics of the atmosphere, and often considered in the

1 models. The mole fraction (shown in Figure 9) was calculated as the ratio between the methane
 2 number density and the sum of the methane number density and the nitrogen number density,
 3 the mayor constituents of the atmosphere. The calculation was limited to the altitudes that were
 4 used to determine temperatures (as explained in Section 2.2) and are shown between dotted
 lines in Figure 7. Our results support the observations of variability and differences in dynamics

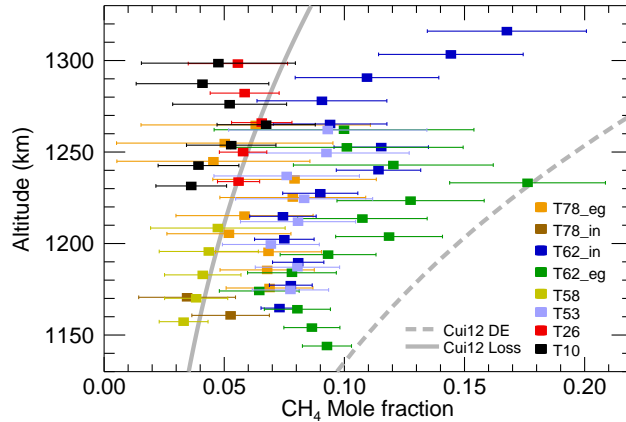


Fig. 9.— Methane mole fraction derived from all solar occultations analyzed. The gray line (Cui12 Loss) represents a model with a loss rate of $3.8 \times 10^{27} s^{-1}$, the blue line (Cui12 DE) represents a diffusive equilibrium model, both from Cui et al. (2012).

5
 6 revealed by the study of Cui et al. (2012). These authors thoroughly revisited the CH_4 structure
 7 in Titan’s upper atmosphere, combining Cassini/INMS data from 32 flybys and incorporating
 8 several updates in the data reduction algorithms. After fixing the eddy mixing profile on the
 9 basis of the ^{40}Ar mole fraction, they used the methane mole fraction derived from INMS data to
 10 constrain the methane escape rate in their model. They found that the considerable variability
 11 in CH_4 structure among different flybys implies that methane escape on Titan is more likely a
 12 sporadic rather than a steady process, with the CH_4 profiles from about half of the flybys showing
 13 evidence for strong escape and most of the other flybys consistent with diffusive equilibrium.
 14 Considering the globally averaged CH_4 mole fraction, the best fit to the data was obtained with a
 15 model using an escape rate of $3.8 \times 10^{27} s^{-1}$. This model profile is shown in Figure 9 (solid line),
 16 together with the one corresponding to diffusive equilibrium conditions (dashed line). The mole
 17 fractions derived from UVIS occultations are all below the diffusive equilibrium model profile,
 18 and most are between the two models, thus confirming the variability of methane escape.

1 Westlake et al. (2014) presented CH_4 mixing ratios derived from Cassini INMS observations
 2 of Titan’s atmosphere from the TA-T95 flybys, which took place from 2004 to 2013. The CH_4
 3 mixing ratio showed a declining trend from mid-2006 to roughly 2008, followed by an upward
 4 trend during the extended solar minimum from 2008 to sometime in 2010. This was followed
 5 by a downward trend in the mixing ratios of CH_4 after the onset of solar maximum conditions
 6 in 2011. Comparing observations from different flybys and through modeling studies using the
 7 time-dependent Titan Global Ionosphere-Thermosphere Model, Westlake et al. (2014) argued that
 8 this trend is due to enhanced photodestruction of CH_4 in Titan’s thermosphere from the increased
 9 solar EUV/UV flux during solar maximum times. The trends observed by Westlake et al. (2014)
 10 are not evident from our methane mole fractions. However, our data set is sparse, and our
 11 uncertainties big, preventing any firm conclusion about the temporal variation of the methane
 12 mixing ratio. On the other hand, most mole fractions derived from UVIS data correspond to
 13 locations and times not covered by INMS data, and can therefore serve as additional constraints
 14 in studies of the methane structure.

15 4.3. Comparison with Other Measurements of Abundance

16 The CH_4 densities and the N_2 densities from UVIS solar occultations presented here
 17 complement the measurements from other instruments (like INMS and UVS), and measurements
 18 from other UVIS observations. Capalbo et al. (2013) showed a synergy between UVIS/EUV-solar
 19 and UVIS/FUV-stellar occultations observed during flyby T53, when the different occultations
 20 provided a measurement of methane number densities at two different, well defined, geographical
 21 coordinates within a time span of some hours. Kammer et al. (2013) analyzed 4 UVIS/EUV-stellar
 22 occultations (flybys T21, T35, T41-I, and T41-II) and derived CH_4 and N_2 number density
 23 profiles between 1000 and 1400 km. The profiles correspond mainly to low/mid latitudes and the
 24 last three fall between those from flybys T26 and T53, presented here. In Figure 10 we compare
 25 the profiles of methane and nitrogen derived from the UVIS/EUV-stellar occultation during T21,
 26 with those we derived from the UVIS/EUV-solar occultation during T26, which took place 88
 27 Earth days later, and further south. Table 3 presents temporal and geographical information

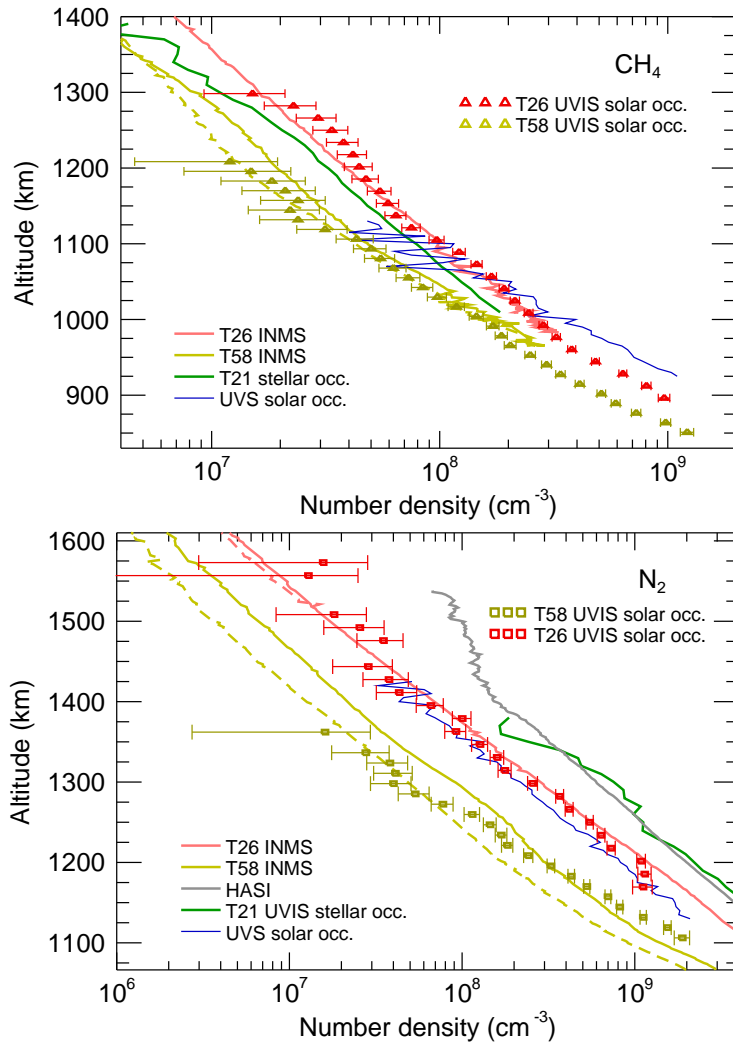


Fig. 10.— Methane (top) and nitrogen (bottom) number density profiles derived from solar occultations T26 (in March 2007) and T58 (in July 2009). Also shown are the profiles for both species measured by UVIS/EUV during a stellar occultation in December 2006 (Kammer et al. 2013), profiles measured by UVS onboard Voyager 1 during a solar occultation in November 1980 (Vervack et al. 2004), the profiles from INMS (inbound: solid line, outbound: dashed line) measured during T26 and T58 (Snowden et al. 2013), and a nitrogen profile calculated from the density measurements performed by the HASI instrument during the Huygens probe descent through Titan’s atmosphere in January 2005 (Fulchignoni et al. 2005).

- 1 for the data in Figure 10. The UVIS/FUV-stellar methane profile from T21 falls below the
- 2 UVIS/EUV-solar profile measured for T26, the FUV-stellar nitrogen profile from T21 is above
- 3 the EUV-solar profile measured for T26.

1 The optimal measurement conditions for INMS and UVIS are different so it is uncommon
2 to have both type of measurements in the same flyby. However, INMS performed measurements
3 of N_2 and CH_4 during flybys T26 and T58. The profiles from the inbound and outbound legs
4 of these flybys are compared with the UVIS solar occultation results in Figure 10. The INMS
5 densities shown were multiplied by the revised calibration factor of 2.2 (Teolis et al. 2015).
6 Assuming no instrumental artifacts or systematic errors, the differences between UVIS and
7 INMS, both measurements corresponding to the same flyby, can be due to spatial variations in
8 the atmosphere. Comparisons of UVIS/EUV-solar occultation results for T53 with INMS, UVS
9 and HASI results were presented in Capalbo et al. (2013). There, the T53 CH_4 densities and N_2
10 densities are compared with corresponding INMS results from the inbound and outbound passes
11 in flybys T51 and T55, that took place about one month before and after T53, respectively.
12 The UVIS/EUV results broadly agreed with most of the results from previous work presented
13 in Capalbo et al. (2013), within factors 1-3 (1-1.8 for comparisons with INMS results). Capalbo
14 et al. (2013) scaled the INMS densities by a factor 2.9 from the original calibration. Using the
15 revised correction factor (Teolis et al. 2015) for the INMS results, makes the UVIS profiles and
16 the INMS profiles in Capalbo et al. (2013) agree within factors 0.8-1.4. The restricted sampling
17 of the available data did not allow the authors to reach a firm conclusion on horizontal/seasonal
18 variations.

19 Also shown in Figure 10 are the N_2 density profile derived from the Huygens Atmospheric
20 Structure Instrument (HASI) mass profile (Fulchignoni et al. 2005), assuming an atmosphere
21 composed of nitrogen and 5% of methane; and the N_2 density and CH_4 density profiles
22 from Vervack et al. (2004) derived from the solar occultation measured by Voyager 1/UVS. The
23 HASI-derived N_2 profile and the profile from the UVIS/EUV-stellar occultation during T21 are
24 above all the other profiles shown. These two are the only profiles measured close to Titan
25 northern winter season, or half way to the Vernal Equinox, all the others were measured close
26 to Titan Vernal Equinox. The UVS profile agrees well with the T26 UVIS/EUV-solar profile,
27 measured almost 27 years later and at higher latitude. Although comparisons with the HASI
28 or the UVS profile could provide clues when analyzing seasonal or long term variations in the
29 atmosphere, no firm conclusions can be made from these specific comparisons.

1 Due to the variety of factors determining the temporal and geographical behavior of the
 2 atmosphere, it is difficult to establish a criterion to compare different profiles from different
 3 observations. Moreover, comparison of results from different experiments is complicated by
 4 differences in retrieval methods or uncertainties in instrument calibration. Nevertheless, the
 5 variability of Titan’s upper atmosphere is undeniable.

6 4.4. Thermospheric Temperature and Temperature Variability

7 Average temperature in the upper atmosphere was calculated from the N_2 number densities
 8 with the procedures described in Section 2.2. The altitude range used for the calculation of
 9 temperature is indicated by the horizontal dotted lines shown in Figure 7. The temperatures
 10 derived from the 8 observations analyzed are shown in Table 1. It is worth noting that
 11 temperatures for the upper atmosphere were not measured before for most of the flybys analyzed
 12 here. We derived two temperatures from the occultation T62_{egress} (see Section 2.2). The lower
 13 limit we obtain is (135 ± 2) K, the ‘low altitude temperature’ we obtain is (179 ± 9) K. The fact
 14 that this temperature was calculated from only the six lower values in the profile (Figure 7) has
 15 to be kept in mind when comparing this temperature with that from other observations.

16 The global average temperature and temperatures for flybys T26 and T58 are shown in
 17 Table 4, together with equivalent results from previous work. We calculated, as a weighted
 18 average, a global temperature of (150 ± 1) K, the standard deviation of the set of 8 values used
 19 is 24 K. These values changed to (149 ± 1) K and 22 K if T62_{egress} is not considered. Our global
 20 temperature is consistent with the global temperatures shown in Table 4 and derived from INMS
 21 data (the value from Westlake et al. (2011) is within $3\text{-}\sigma$ from our value). It should be noted
 22 that our global average was determined from only 8 values. The other references in Table 4 use
 23 temperatures determined from several tens of flybys.

24 Interestingly, our temperature for flyby T58 is remarkably cold in comparison with the others
 25 in Table 4. It should be noted that the INMS measurements correspond to the mid/high southern
 26 latitudes while our measurement corresponds to 86 N, nearly at the north pole. For T26, on the
 27 contrary, our temperature is consistent with the ones presented in the table. Using a similar

Table 3. Temporal and geographical characteristics for the set of measurements shown in Figure 10.

Measurement	Time (mm/yy)	Close to Titan Season	Solar Activity	Latitude ^a (deg)	Longitude ^a (deg W)
UVIS T53 solar occ.	04/09	Vernal Equinox	Min.	-21 – -29	237
UVIS T53 star occ.	04/09	Vernal Equinox	Min.	38 – 39	294 – 308
UVIS T26 solar occ.	03/07	Vernal Equinox	Low	-76 – -77	41 – 29
UVIS T58 solar occ.	07/09	Vernal Equinox	Low	87 – 85	240 – 237
UVIS T21 star occ.	12/06	North. win./Ver. Eq.	Low	-35	116
HASI	01/05	Northern winter	Low	-9.5	186.2
UVS solar occ.	11/80	Vernal Equinox	High	4	107
INMS T26	03/07	Vernal Equinox	Low	31.7	358
INMS T58	07/09	Vernal Equinox	Low	-52.2	178

^aFor INMS observations, the latitude and longitude correspond to closest approach.

Table 4. Global temperature and temperatures for specific flybys.

Reference	This Work	Cui et al. (2009)	Westlake et al. (2011)	Snowden et al. (2013)
Global average (K)	150 ± 1	151.0 ± 0.5	153.0 ± 1.2	150.7 ± 4.2
T26 (K)	139 ± 5	...	142.9 ± 1.3	141.0 ± 6.5 / 138.2 ± 4.9 ^b
T58 (K)	113 ± 3	...	~140 ^a	156.5 ± 5.5 / 145.6 ± 6.3 ^b
Instrument	UVIS	INMS	INMS	INMS

^aApproximate value from Figure 4 in the reference.

^bInbound/outbound leg, high altitude density level.

1 technique as the one presented here, Kammer et al. (2013) derived averaged temperature for the
 2 upper atmosphere from the N_2 profiles measured during UVIS/EUV-stellar occultations. Their
 3 value for T21 is $(149.6^{+13.6}_{-11.6})$ K, which falls between the 163 K we derived from T10 and the 139 K
 4 we derived from T26. Also fitting isothermal profiles to the nitrogen densities, Vervack et al.
 5 (2004) found a thermospheric temperature of (153 ± 5) K with no variation, taking into account
 6 the uncertainties, for the ingress and egress occultations measured by Voyager 1/UVS in 1980.
 7 The comparison of values from individual flybys makes sense only when factors such as location
 8 and time are also taken into account, as they affect the thermospheric temperature. Nevertheless,
 9 the average temperature that we retrieved from Cassini/UVIS solar occultations agrees with all
 10 previous measurements, based either on Cassini/INMS, Voyager/UVS or Cassini/UVIS stellar
 11 occultations. The range of temperatures we obtained also agrees with the previously determined
 12 range of temperatures, including the peculiarly cold and warm flybys, thus confirming the
 13 remarkable variability that the INMS has observed.

14 Variability is important in Titan’s atmosphere. Measured temperatures can vary roughly
 15 between 100 - 200 K (see for example Snowden et al. 2013) from flyby to flyby. The combined
 16 effects from the different variables affecting the behavior of the atmosphere (day/night, season,
 17 position in the magnetosphere, etc.) are complex and the variables cannot be easily decoupled,
 18 especially when dealing with limited data sets with poor statistics and easily biased by outliers,
 19 like in the present case. Nevertheless, an evident correlation of our 8 temperatures with some of
 20 those variables could suggest a trend in behavior. We present next the temperatures as a function
 21 of several variables, concentrating first in the horizontal variability and, later, in the temporal
 22 variability.

23 Figure 11 shows the temperatures from all the solar occultations as a function of latitude
 24 (left) and longitude (right). The temperatures decrease from the equator to the north pole. This
 25 trend does not repeat in the southern hemisphere, where mid-latitude temperatures from the
 26 flybys T10 and T62_{egress} are warmer than that derived for a high-latitude from the T53 flyby.
 27 We remind however that the lower limit we derived for the temperature for T62_{egress} is 135 K.
 28 No correlation with longitude is evident from the right plot in Figure 11. In particular, three
 29 different values spanning almost the whole range of temperature measured are concentrated in the

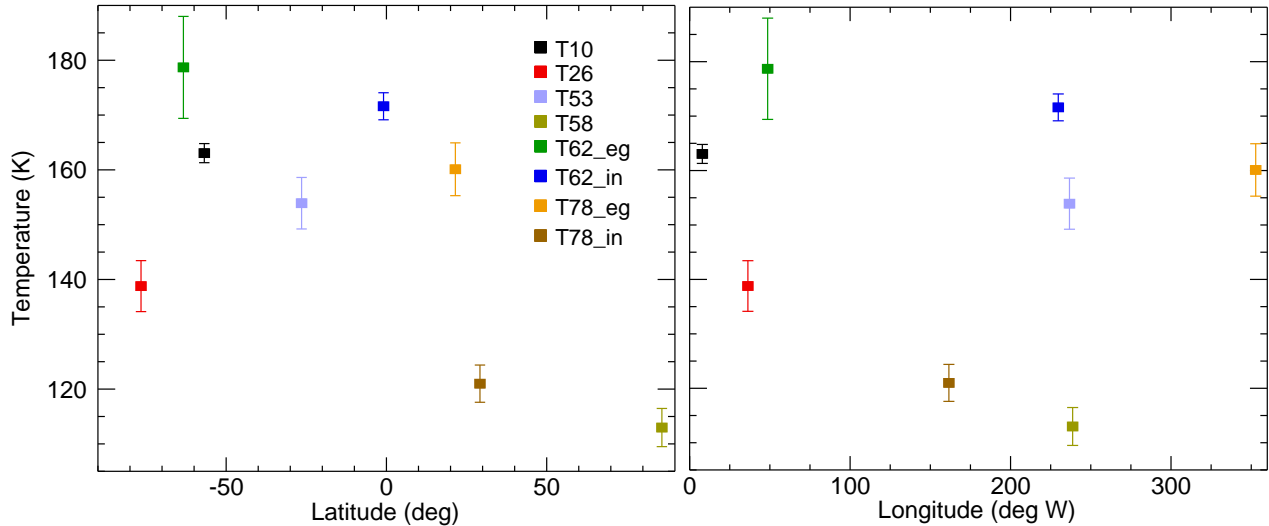


Fig. 11.— Upper atmospheric temperatures as a function of latitude (left) and longitude (right) for the solar occultations analyzed.

1 region 230° - 240° W. Cui et al. (2009) studied composition and thermal structure of the upper
2 atmosphere based on the analysis of INMS data from 15 Titan flybys spanning 2.5 years, from
3 April 2005 till November 2007. They showed that the equatorial region in Titan’s thermosphere
4 appears to be warmer than the north polar region. Cui et al. (2009) give a temperature difference
5 between the equator and north pole of ~ 10 K, while the difference between our northernmost
6 temperature and the one closer to the equator is of about 60 K. The restricted sampling of the
7 available INMS data at the time of publication did not allow Cui et al. (2009) to make a firm
8 conclusion on the realistic horizontal variations. Later work relying on a much larger number of
9 INMS measurements include that of Westlake et al. (2011) (29 flybys from 2004 till 2009) and
10 that of Snowden et al. (2013) (32 flybys from 2006 till 2010). Both have pointed to the same
11 trend — that the north polar region tends to have the lowest temperatures while the equator
12 has the warmest temperatures. This trend does not appear to hold in the southern hemisphere,
13 however, where the mid-latitude region tend to be warmer than the low latitude region. This is
14 consistent with our measurements. Snowden et al. (2013) found an insignificant difference in the
15 temperature calculated for different longitude regions.

16 The lack of sufficient data points prevents firm conclusions about horizontal variability.

1 Although this is particularly true for our sparse sampling of the atmosphere from solar
2 occultations, we present results for flybys not included in the studies cited above, so our works
3 are complementary. The data suggest that there is no detectable correlation with longitude. On
4 the other hand the north pole might be colder than the equator or southern latitudes, this calls
5 for further attention to this latitudinal trend in thermospheric temperatures.

6 Titan’s atmosphere presents also temporal variability. The temperatures from the
7 solar occultations correspond to either the morning or evening terminator (See Figure 12).
8 Measurements in the morning terminator could be considered representative of an atmosphere
9 coming out the night, and those from the evening terminator representative of an atmosphere
10 coming from a day period. No day/night differences are evident in our results, measurements in the
11 evening terminator span across almost the whole range of temperature measured. Mueller-Wodarg
12 et al. (2000), using a 3-D General Circulation Model (GCM) of Titan’s thermosphere, found
13 diurnal and hemispheric variability of up to 10 - 20 K in thermospheric temperatures, resulting
14 from solar EUV heating; the variability was largest above 1300 km. On the contrary, Cui et al.
15 (2009) found the nightside to be warmer than the dayside. A similar trend was found in Westlake
16 et al. (2011) and Snowden et al. (2013); although the day/night temperature difference found by
17 the latter is smaller than in previous calculations, and their final conclusion is that no relevant
18 dependence on local time can be derived from the observations, in agreement with our results
19 from the UVIS occultations.

20 Figure 12 shows the measured temperatures as a function of time, the vertical line showing
21 Titan’s Vernal Equinox on 2009 August 11. No correlation with time or Solar activity is apparent,
22 as neither is from the temporal trend shown in Westlake et al. (2011). Snowden et al. (2013) state
23 that the average temperature of Titan’s thermosphere may have decreased by about 10 - 15 K
24 around mid-2007, or around T32. However, the data from the solar occultations are not sufficient
25 to establish any long term temperature trends in the data.

26 Titan’s thermospheric temperature vary considerably as a function of time and location, yet,
27 this variability might result from a combined effect of the variables considered here, and taking
28 only one of them at a time could be misleading.

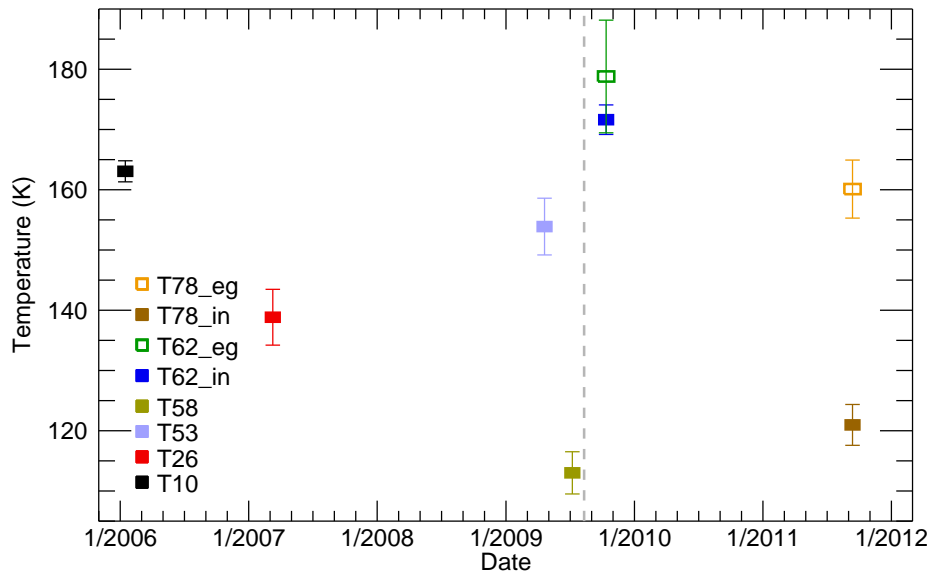


Fig. 12.— Upper atmospheric temperatures as a function of time, corresponding to the morning terminator (open symbols) or the evening terminator (closed symbols). The vertical line shows Titan’s Vernal Equinox in August 2009. Date format: M/YYYY.

5. SUMMARY AND CONCLUSIONS

1

2 We analyzed 8 UVIS/EUV-solar occultations by Titan’s atmosphere, taking place between
 3 flybys T10 and T78, for which data are available in the PDS archive. We developed methods
 4 to correct the data from background contamination, and wavelength shifts due to pointing
 5 instabilities. In some cases, the wavelength re-calibration implemented permitted the analysis
 6 of observations that, without the corrections, would be useless for retrieving the atmospheric
 7 composition.

8 From the solar occultations we retrieved the density profiles of CH_4 at altitudes of 850-
 9 1300 km, and density profiles of N_2 at altitudes of 1100-1600 km. The profiles include oscillations
 10 that might be indicative of atmospheric waves (Koskinen et al. 2011; Snowden et al. 2013) or,
 11 in case of small scale fluctuations, artifacts from the inversion procedure. We used the density
 12 profiles to calculate the CH_4 mole fractions. The results come with relatively large uncertainties,
 13 but they appear to confirm the variability of CH_4 mixing ratio and the variability of methane
 14 escape observed in the INMS data (Cui et al. 2012; Westlake et al. 2014).

1 The data presented here complement measurements from other instruments. In Section 4.3
2 we compared our CH₄ profiles and N₂ profiles with those from other observations and instruments.
3 These data cover a wide range of locations and times. We stress the difficulty of comparing the
4 different profiles, which are affected by different factors determining the undeniable variability
5 of the atmosphere. We addressed this variability in terms of an analysis of number density
6 variation and thermospheric temperature variation. The data set of solar occultations analyzed
7 cover different latitudes and longitudes, in many cases corresponding to times and locations
8 for which no experimental thermospheric temperatures were available in the bibliography. The
9 previously observed variability of CH₄ abundances and N₂ abundances in the upper atmosphere
10 is confirmed by the difference between profiles from different solar occultations, or among the
11 profiles presented here and those derived from other observations at different times/locations. In
12 particular, in agreement with INMS observations, we observed an overall tendency of decreasing
13 abundance with time for both species, the abundances measured late in the Cassini mission being
14 smaller than those measured early in the mission.

15 The upper atmosphere temperature was calculated for each of the 8 solar occultations
16 analyzed. Our global mean temperature of (150 ± 1) K agrees with previous measurements
17 by different instruments. The range of temperatures we obtained agrees with the previously
18 determined range of temperatures, including the peculiarly cold and warm flybys. Analysis of
19 the eight temperatures as a function of different geographical and temporal variables showed no
20 evident correlation with longitude, local time or season. The data suggest that the north pole
21 might be colder than the equator or southern latitudes, although the lack of sufficient data points
22 prevents firm conclusions in this regard.

23 The variability in the densities and in thermospheric temperature is undeniable. However,
24 the sampling of the occultations data set is restricted, uncertainties from different profiles overlap
25 at high altitudes, and different locations are blended in the statistical analysis of number densities.
26 Thus, the general trends presented should be interpreted with caution. Moreover, we stress the
27 fact that the variability observed might be caused by a complex combination of the variables
28 considered (or other not considered) in the analysis of temperature variability, making these kind
29 of studies very delicate.

1 In summary, the number density profiles, mole fraction profiles, and temperatures presented
2 provide new observational data to constrain the studies of composition, temperature, and
3 dynamics of Titan’s upper atmosphere. Furthermore, Cassini arrived at the Saturnian system in
4 2004 and the mission is planned to be continued till 2017, so more observations will be available
5 to deepen the study of variability and long-term changes in Titan’s atmosphere.

6 We acknowledge the financial support from the French Space Agency (Centre National
7 d’Études Spatiales, CNES). TTK was supported by the NASA CDAPS grant NNX14AD51G.

REFERENCES

- 1
- 2 Acton, C. H. 1996, *Planet. Space Sci.*, 44, 65
- 3 Broadfoot, A., et al. 1977, *Space Sci. Rev.*, 21, 183
- 4 Capalbo, F. J. 2014, PhD thesis, University of Paris Est
- 5 Capalbo, F. J., Bénilan, Y., Yelle, R. V., et al. 2013, *ApJ*, 766, L16
- 6 Cui, J., Yelle, R. V., Strobel, D. F., et al. 2012, *J. Geophys. Res.*, 117, E11006
- 7 Cui, J., Yelle, R. V., Vuitton, V., et al. 2009, *Icarus*, 200, 581
- 8 Fulchignoni, M., et al. 2005, *Nature*, 438, 785, doi:10.1038/nature04314
- 9 García-Comas, M., López-Puertas, M., Funke, B., et al. 2011, *Icarus*, 214, 571
- 10 Kameta, K., Kouchi, N., Ukai, M., & Hatano, Y. 2002, *J. Electron Spectrosc. Relat. Phenom.*,
11 123, 225
- 12 Kammer, J., Shemansky, D., Zhang, X., & Yung, Y. 2013, *Planet. Space Sci.*, 88, 86 , atmospheres,
13 Magnetospheres and Surfaces of the outer planets, their satellites and ring systems: Part
14 {IX}
- 15 Koskinen, T., Yelle, R., Snowden, D., et al. 2011, *Icarus*, 216, 507
- 16 Lara, L. M., Lellouch, E., Lopez-Moreno, J. J., & Rodrigo, R. 1996, *J. Geophys. Res.*, 101, 23261
- 17 LASP. 2014, *Cassini UVIS User’s Guide.*, Laboratory for Atmospheric and Space Physics,
18 Boulder, CO, <http://pds-rings.seti.org/cassini/uvis/index.html>
- 19 Lavvas, P., Sander, M., Kraft, M., & Imanaka, H. 2011, *ApJ*, 728, 80
- 20 Lewis, B. R., Heays, A. N., Gibson, S. T., Lefebvre-Brion, H., & Lefebvre, R. 2008, *J. Chem. Phys.*,
21 129, 10.1063/1.2990656
- 22 Magee, B. A., Waite, J. H., Mandt, K. E., et al. 2009, *Planet. Space Sci.*, 57, 1895

- 1 Mueller-Wodarg, I., Yelle, R., Mendillo, M., Young, L., & Aylward, A. 2000, *J. Geophys. Res.*,
2 105, 20833
- 3 Mueller-Wodarg, I. C. F., Yelle, R. V., Cui, J., & Waite, J. H. 2008, *J. Geophys. Res.*, 113,
4 E10005
- 5 Samson, J. A. R., Masuoka, T., Pareek, P. N., & Angel, G. C. 1987, *J. Chem. Phys.*, 86, 6128
- 6 Sarani, S. 2009, in *Proceedings of the AIAA Guidance, Navigation, and Control Conference* (New
7 York: Am. Inst. of Aeronaut. and Astronaut.), abstr. 5763
- 8 Smith, G. R., & Hunten, D. M. 1990, *Reviews of Geophysics*, 28, 117
- 9 Smith, G. R., Strobel, D. F., Broadfoot, A. L., et al. 1982, *J. Geophys. Res.*, 87, 1351
- 10 Snowden, D., Yelle, R., Cui, J., et al. 2013, *Icarus*, 226, 552
- 11 Stevens, M. H., Evans, J. S., Lumpe, J., et al. 2015, *Icarus*, 247, 301
- 12 Stevens, M. H., Gustin, J., Ajello, J. M., et al. 2011, *J. Geophys. Res.*, 116, A05304
- 13 Strobel, D. F., Summers, M. E., & Zhu, X. 1992, *Icarus*, 512
- 14 Teolis, B., Niemann, H., Waite, J., et al. 2015, *Space Sci. Rev.*, 1
- 15 Vervack, J. R. J., Sandel, B. R., & Strobel, D. F. 2004, *Icarus*, 170, 91
- 16 Waite, J.H., J., Niemann, H., Yelle, R., et al. 2005, *Science*, 308, 982
- 17 Westlake, J. H., Bell, J. M., Waite, J. H., et al. 2011, *J. Geophys. Res.*, 116, A03318
- 18 Westlake, J. H., Waite, J. H., Bell, J. M., & Perryman, R. 2014, *J. Geophys. Res.*, 119, 8586
- 19 Yelle, R. V., Cui, J., & Mueller-Wodarg, I. C. F. 2008, *J. Geophys. Res.*, 113, E10003
- 20 Yelle, R. V., Strobell, D. F., Lellouch, E., & Gautier, D. 1997, in *Huygens: Science, Payload and*
21 *Mission, Proceedings of an ESA conference*, ed. A. Wilson, 243 – 256, eSA SP-1177
- 22 Yung, Y., Allen, M., & Pinto, J. 1984, *ApJS*, 55, 465

